Proceedings of the ASME 2013 32nd International Conference on Ocean, Offshore and Arctic Engineering
OMAE2013
June 9-14, 2013, Nantes, France

OMAE2013-10120

HYDRODYNAMIC MODELING OF TENSION LEG PLATFORM WIND TURBINES

Erin E. Bachynski*
Center for Ships and Ocean Structures
Norwegian University of Science and Technology
Trondheim, Norway 7491
Email: erin.bachynski@ntnu.no

Torgeir Moan
Center for Ships and Ocean Structures
Norwegian University of Science and Technology
Trondheim, Norway 7491
Email: torgeir.moan@ntnu.no

ABSTRACT

In order to compute the system response of tension leg platform wind turbines (TLPWTs), it is important to accurately capture the hydrodynamic loading not only at the wave frequency, but also in the low (difference) and high (sum) frequency ranges. The current work compares the dynamic response of several single column TLPWT designs in different wind and wave conditions using three hydrodynamic models: first order potential flow with viscous drag, first and second order potential flow with viscous drag, and a Morison's equation model. Second order wave forces were found to have a relatively small effect on the structural load predictions: increased tendon tension variation of approximately 2-10% was observed in storm conditions, while negligible effects were observed in operational conditions. The Morison model, however, gave significantly larger pitch forcing near the natural period, leading to larger structural load predictions in all sea states.

INTRODUCTION

Tension leg platform wind turbine (TLPWT) and taut leg buoy concepts are promising for intermediate water depths, since the limited platform motions are expected to reduce the structural loading on the tower and blades compared to other floating concepts, without requiring the large draft of a spar or spread mooring system of a semi-submersible [1–3]. In order to minimize first order wave loading, the natural periods of a TLPWT design are typically very short for the vertical plane motions (heave, roll, pitch) and quite long for the horizontal plane motions (surge, sway, yaw). In order to compute the system response, it is therefore important to accurately capture the hydrodynamic loading not only at the wave frequency, but also in the sum- and difference-frequency ranges.

Existing independent 5 MW TLPWT designs include designs from Concept Marine Associates (CMA) [4], the Massachusetts Institute of Technology and the Italian Enel group (MIT/Enel) [3], MIT and the National Renewable Energy Laboratory (MIT/NREL) [5,6], the University of Maine [2,7], Glosten Associates [8], GL Garrad Hassan [9], a Japanese collaboration (Nihei et al.) [10], and IDEAS [11]. These designs represent a wide range of displacements (Δ) from 846 tonnes [10] to 12,187 tonnes [5], with stiffness provided by 3 to 8 tendons, and waterline diameter between 4.5 and 18 m. Published estimates of surge natural periods for these designs range from approximately 25 [9] to 60 s [5], while the heave natural period is between 1.0 [7] and 2.3 s [5]. The coupled platform pitch and tower bending mode is typically found to be between 3.5 and 4.5 s.

Due to the wide range of designs, different hydrodynamic models may be appropriate for different platforms. Linear potential theory is typically used for the analysis of large volume structures, while slender elements may be modeled using Morison's equation, as long as the wave velocity in the free surface zone is appropriately modeled [12]. Although a previous study of a semi-submersible wind turbine structure with 10 m characteristic length at the waterline indicated that the Morison formulation, with coefficients chosen based on the potential flow results, could be used to obtain similar structural responses in the turbine and mooring system [13], a similar study for a TLPWTs has not been carried out previously.

*Address all correspondence to this author.

In addition to the nonlinearity introduced by the quadratic viscous drag force, nonlinear low- and high-frequency wave forces arise due to the quadratic term in Bernoulli's equation and the evaluation of pressures at the exact body position [14]. Experience from the oil and gas industry indicates that both slow drift motions and high-frequency motions induced by second order wave forces may be important for computing the mooring loads of large volume structures. In particular, early investigation into the second order forcing on a TLP indicated that the spectrum and RMS of tendon tensions predicted by including the nonlinear effects could be 2 to 3 times greater than first order approximations [15]. Furthermore, Roald et al. suggested that second order sum-frequency forces may also be important for TLPWTs [16].

TLPWTs are somewhat smaller than traditional oil and gas TLPs, and the structural responses depend not only on hydrodynamics but also on the wind forces and control system. Furthermore, some wind turbine analysis codes are limited to Morison's equation for the computation of wave loads, and very few are able to include the second order high-frequency loads. Therefore, a better understanding of the sensitivity of the global response to the hydrodynamic modeling is required. This study used the Simo-Riflex-AeroDyn coupled software in order to examine the effect of three hydrodynamic models on the response of several representative TLPWT structures.

TLPWT MODELS

Four TLPWT models for 150 m water depth are considered here. Fig. 1 and Table 1 describe the four designs, which have been previously studied using first order potential forces and viscous drag in [17].

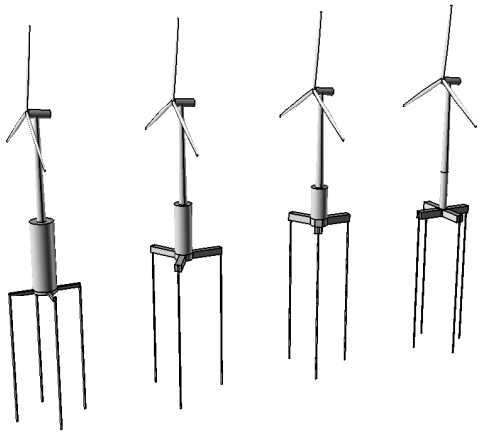

FIGURE 1. TLPWT DESIGNS 1-4

The diameter at the waterline ranges from 18.0 m (TLPWT 1) to 6.5 m (TLPWT 4). Diffraction effects are therefore not expected to be important for any of the designs for waves longer than approximately 9 s, indicating that Morison's equation may be reasonable to apply for most North Sea conditions.

The natural periods of the TLPWTs are given in Table 2. Decay tests of the finite element model, with parked rotor, were used to compute the natural periods using the potential theory added mass and the selected added mass coefficients for the Morison's model (described in greater detail in the following section). Good overall agreement was obtained for the natural periods, which, except for yaw, are outside of the expected first order wave excitation. The pitch/bending modes represent a combination of platform pitch and tower bending, and are very similar for all of the platforms. An increase in the second pitch/bend period using the distributed added mass of the Morison model was observed for all platforms, particularly TLPWT 1 (with the largest draft).

HYDRODYNAMIC MODELS

Three hydrodynamic models, given below, are considered for the TLPWT platforms:

1. P1+V: first order potential flow and viscous drag,
2. P2+V: first and second order potential flow and viscous drag,
3. M: Morison formulation (Froude-Krylov and viscous drag).

The considerations included in the different models are summarized in Table 3. Both the P1+V and P2+V formulations include mean drift forces using the Newman approximation, which depends only on first order information [12]. Neither the detailed slowly-varying QTF nor the slowly-varying wave-drift damping are modeled here.

Identical transverse viscous damping coefficients are used in all three hydrodynamic models: $C_D = 0.7$ (see Eq. 3) for both circular cross sections with diameter D and square cross sections (using the width as the representative length). Although this assumption may underpredict the drag on the square cross sections, it is taken as a reasonable first approximation based on Reynolds and Keulegan-Carpenter number [12].

In all cases, the wave forces on the hull and tendons were computed at the static position of the TLPWT. Viscous and Morison inertia forces were computed up to the instantaneous water level, based on wave kinematics at the platform's original position, using a constant incident wave potential above the still water line.

First Order Potential with Morison Drag

Linear wave theory is sufficient to describe the dominant wave loading on many offshore structures [12]. Using, for example, a source distribution technique, the first order velocity potential $\Phi^{(1)}$ can be obtained for a general shape in the absence of current. As shown in Eq. 1, the time dependence of first order results is the same as the incoming wave frequency, ω_j.

$$\Phi^{(1)}(x,t) = \mathrm{Re}\sum_j \phi_j^{(1)}(x)e^{i\omega_j t} \tag{1}$$

TABLE 1. TLPWT DESIGNS

	TLPWT 1	TLPWT 2	TLPWT 3	TLPWT 4
Diameter (m)	18.0	14.0	14.0	6.5/10.0
Draft (m)	45.0	35.0	22.0	29.0
Pontoon radius (m)	27.0	32.0	28.0	25.0
Pontoon height/width (m)	2.4/2.4	5.0/5.0	6.0/6.0	6.0/6.0
Tendon diameter (m)	1.4	1.1	1.3	1.2
Tendon thickness (mm)	46.2	36.3	42.9	39.6
Displacement (m^3)	11 866	7 263	5 655	4 114
Steel mass (tonnes)	2 322	1518	1293	859
Concrete ballast (tonnes)	6456	3314	1389	506
Tendon pretension (kN)	6 868	4 963	8 262	5 556

TABLE 2. DAMPED NATURAL PERIODS, INCLUDING TOWER FLEXIBILITY, BASED ON DECAY TESTS OF THE FE MODEL WITH PARKED ROTOR AND NO WAVES.

	TLPWT 1		TLPWT 2		TLPWT 3		TLPWT 4	
	P1+V	M	P1+V	M	P1+V	M	P1+V	M
Surge (s)	55.78	55.86	53.13	52.12	41.86	41.77	34.22	34.39
Heave (s)	0.55	0.55	0.75	0.75	0.60	0.60	0.53	0.57
Pitch/ Bend (1) (s)	2.79	2.80	2.81	2.81	2.76	2.78	2.74	2.75
Pitch/ Bend (2) (s)	0.51	0.60	0.48	0.51	0.39	0.40	0.39	0.40
Yaw (s)	13.99	14.00	18.06	18.22	18.63	18.62	19.71	20.24

The solution for the velocity potential gives the frequency-dependent added mass ($A_{ij}(\omega)$), linear damping ($B_{ij}(\omega)$), and wave excitation ($X_j(\omega)$) [12]. The first order potential for each TLPWT hull was computed using the 3D panel capability in the Wadam software, which is based on the well-known WAMIT software [18]. In the case of TLPWT 1, the pontoons were not included in the potential flow model, leading to near zero yaw added mass. All other TLPWT potential flow models included the pontoons. The added mass and damping coefficients obtained for each TLPWT hull are shown in Figs. 2 and 3.

As shown, there is some frequency variation in the surge added mass coefficients, and more significant frequency dependence in the damping coefficients. The linear radiation damping is small compared to the quadratic viscous damping added to the model using the Morison formulation, and approaches zero for both high and low frequencies.

Second Order Sum-Frequency Potential with Morison Drag

There are several contributions to nonlinear forcing on large volume offshore structures: relative vertical motion between the structure and waves, the quadratic term in Bernoulli's equation, and the computation of wave loads at the instantaneous position of the body [14].

For plane waves, the full second order potential includes both sum-frequency (ϕ_{jl}^{+}) and difference-frequency (ϕ_{jl}^{-}) components, as in Eq. 2, where combinations of wave frequencies ω_j and ω_l are considered [15].

$$\Phi^{(2)}(x,t) = \mathrm{Re}\sum_j \sum_l \left[\phi_{jl}^{+}(x)e^{i(\omega_j+\omega_l)t} + \phi_{jl}^{-}(x)e^{i(\omega_j-\omega_l)t}\right] \tag{2}$$

Although the second order difference-frequency forces may affect the low-frequency motions of the TLPWT, this work does not consider the full difference-frequency quadratic transfer function (QTF). Instead, the Newman approximation [12] is applied, and only the diagonal terms of the difference-frequency QTF (which can be obtained from the first order potential) are used due to limitations in the SIMO QTF implementation. The applied Newman approximation is expected to underpredict the forces based on the full QTF, but the wind forcing at these frequencies dominates the wave forcing [16].

The sum-frequency forces on a TLPWT may be important

TABLE 3. CONSIDERATIONS INCLUDED IN THE HYDRODYNAMIC MODELS

	P1+V	P2+V	M
Added Mass	freq.-dep.	freq.-dep.	constant
Linear Damping	freq.-dep.	freq.-dep.	not modeled
Quadratic Damping	Morison	Morison	Morison
1st Order Wave Excit.	rad. + diff.	rad. + diff.	inertia
Sum-Freq. QTF	not modeled	direct method	not modeled
Diff.-Freq. QTF	not modeled	not modeled	not modeled
Mean Wave Drift Forces/Mom.	Newman approx. + Viscous	Newman approx. + Viscous	Viscous

for accurate prediction of vertical plane motions and tendon tension. The sum-frequency pressure variation decays very slowly with depth, particularly for small frequency differences [12]. Although the contribution from the quadratic term in Bernoulli's equation can be computed from the first order results, it has been shown that it is nonconservative to consider only this effect; that is, it is necessary to compute the second order potential to obtain accurate forcing estimates [19, 20].

The boundary value problem that must be solved to find $\phi_{jl}^{+}(x)$ presents a particular computational challenge: the free-surface forcing term. This term decreases slowly with distance away from the body and includes products of highly oscillatory terms [15]. The tool used here for computing $\Phi^{(2)}(x,t)$ was WADAM, which has a particular limitation: there may only be 3000 free surface panels in the basic part of the model (ie, one quadrant for double-symmetric hulls, or two quadrants for hulls with a single plane of symmetry) [18].

DNV recommends 6 TLPWT hull panels per second-order wavelength [21]. For panels with diagonal dimension 0.5m, this implies greatest confidence in results for incoming waves with periods of at least 5.5s. The shortest wave periods included in the second order analysis were 4.5s. Finer meshing around corners and the waterline [21] was achieved by non-uniform edge element distributions.

For the free surface mesh, the partitioning radius R_2 must enclose the hydro model, and $R_2 \approx O(H)$ for shallow water and $R_2 \approx O(\lambda)$ for deep water, where H is the water depth and λ is the wavelength [18]. It has been observed that, for the ISSC TLP, the convergence of the heave force was relatively slow with respect to R_2, as compared to surge and pitch components [20].

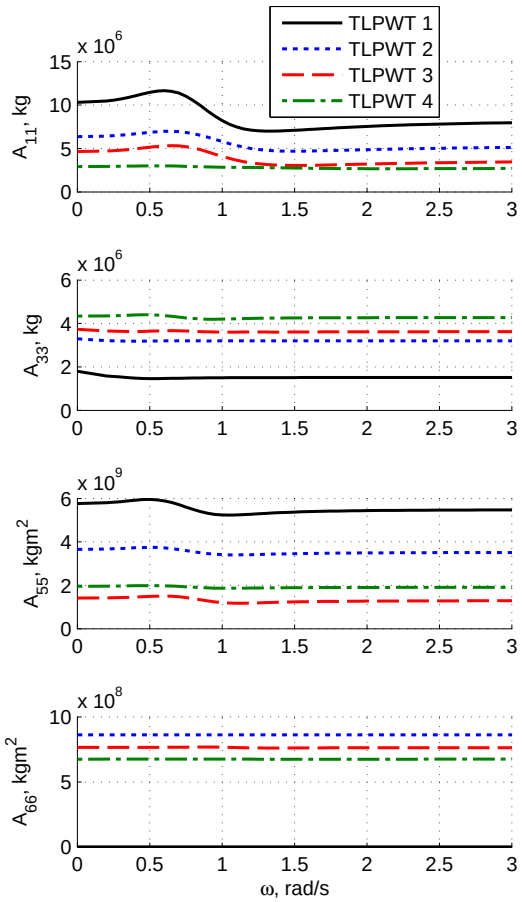

FIGURE 2. ADDED MASS COEFFICIENTS IN SURGE, HEAVE, PITCH, AND YAW

After performing a convergence study for R_2 and the diameter at the waterline, free surface meshes for each TLPWT were chosen to give the best possible results for both long and short waves within the software limitation. The water depth considered here is $H = 150$ m, which can be considered deep water for waves shorter than approximately 14 s, or intermediate water depth for longer waves. Using $R_2 = 150$ m gave sufficiently good results for long waves, and the diagonal dimension at the structural waterline was always less than 1.0 m.

Figs. 4 and 5 show the sum-frequency pitch moment QTFs for TLPWTs 1 and 3, respectively. The first pitch-bend frequency is shown as a dashed line. As shown, the QTF tends to increase for increasing frequencies, and the trough along the diagonal for low frequencies is more pronounced when large pontoons are present.

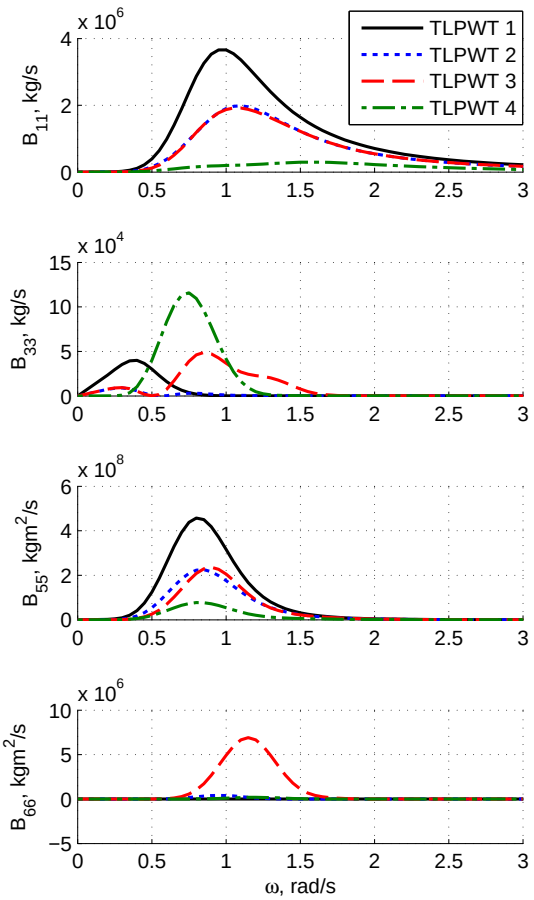

FIGURE 3. RADIATION DAMPING COEFFICIENTS IN SURGE, HEAVE, PITCH, AND YAW

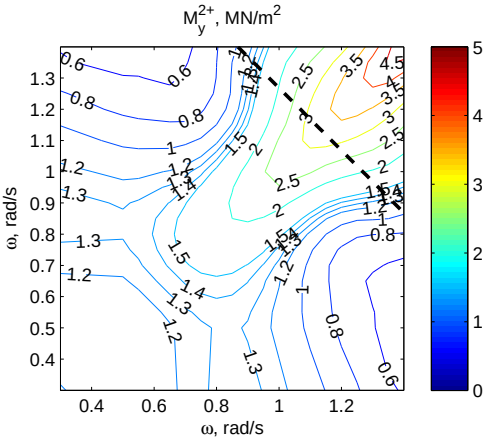

FIGURE 4. SUM-FREQUENCY PITCH FORCE QTF, TLPWT 1. DASHED LINE INDICATES FIRST PITCH-BENDING FREQUENCY.

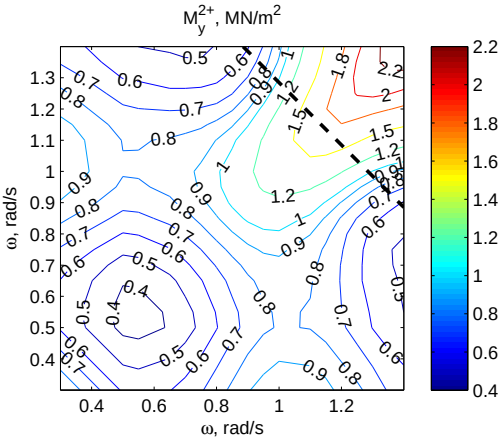

FIGURE 5. SUM-FREQUENCY PITCH FORCE QTF, TLPWT 3. DASHED LINE INDICATES FIRST PITCH-BENDING FREQUENCY.

Morison Formulation

Morison's equation is often used for slender structures where the diameter D is small compared to the wavelength λ (roughly, $D < \lambda/5$) [12]. The transverse force per length (f) on a vertical cylindrical section is given by Eq. 3, where $C_a = C_m - 1$ is the added mass coefficient, C_D is the drag coefficient, u is the transverse wave particle velocity, and v is the local transverse body velocity.

$$f = \rho\pi\frac{D^2}{4}\dot{u} + \rho C_a \pi \frac{D^2}{4}(\dot{u}-\dot{v}) + \frac{1}{2}\rho C_D D\,(u-v)\,|u-v| \quad (3)$$

The first term in Eq. 3 represents the Froude-Krylov force; the second term includes the added mass contributions; and the final term represents the viscous drag forces. According to the deep water limit of linear wave theory, at a depth z, the horizontal water particle acceleration due to wave component j is given by Eq. 4, where ω_j is the wave angular frequency, ζ is the wave amplitude, $k = 2\pi/\lambda$ is the wave number, and ϕ_j is the component phase angle.

$$\dot{u} = \omega^2 \zeta e^{kz} \cos\left(\omega_j t - kx + \phi_j\right) \quad (4)$$

Assuming deep water ($\omega^2 = gk$) and neglecting $\dot{v}$, a transfer function (H_{Mor}) for the Froude-Krylov and added mass forces on a section of length dl centered at depth z is given by Eq. 5.

$$H_{Mor} = \frac{f}{\zeta} \approx \rho V(1+C_a)\omega^2 e^{(\omega^2 z/g)} \quad (5)$$

Noting that the z-coordinate will always be negative, the dependence on ω is $H_{Mor} \propto \omega^2/e^{\alpha\omega^2}$, where α is a positive constant

value for a given depth. Since this function may not decay at the same rate as the excitation force obtained from potential flow theory for high frequencies, the model may predict significantly different responses.

When using a Morison model, it is important to correctly include the dynamic pressure term on vertical elements (see for example [13]). In the Morison model, the dynamic pressure and the vertical added mass on the center column were included through an extra element at the keel.

Force Transfer Functions

The primary first order force contribution for a single-column TLP comes from the Froude-Krylov and inertia forces on the main column. The representation of the forcing on the main column (neglecting viscous damping and body acceleration) for the Morison and potential flow models can differ significantly in the high-frequency range, as shown in Figs. 6(a)-6(b), for surge and pitch, respectively. Theoretical results were obtained from the potential flow solution and Eq. 5, while simulation results in the wave frequency range are obtained from simulations with $H_s = 2.5$m, $T_p = 9.8$s. The difference in surge forcing is not of great importance for the structural response, since the surge natural frequency is lower than the wave frequency, also excited by the turbulent wind, and relatively unimportant for mooring system loads. The pitch/bending natural frequency is close to 2.25 rad/s, where there is a large difference in the forcing and very little hydrodynamic damping. The pitch/bending response is important for the tower bending loads and the variations in tendon tension: despite the relatively small ocean wave energy at this frequency, the large difference in force transfer function may lead to differences in the computed structural response.

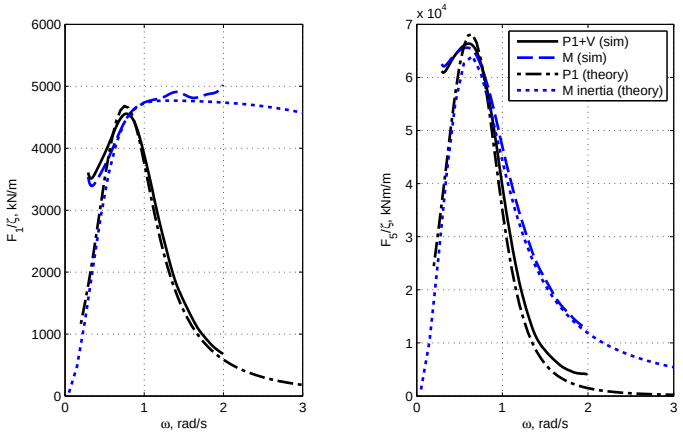

(a) SURGE (b) PITCH

FIGURE 6. WAVE FORCE TRANSFER FUNCTION, TLPWT 1.

GLOBAL ANALYSIS

Three computer codes were used to model the coupled behavior of the TLPWT systems in the time domain: Simo, which models the rigid body hydrodynamics of the hull [22]; Riflex, which includes the finite element solver, flexible elements for the tendons, tower, shaft, and blades, and the link to an external controller [23]; and AeroDyn, which provides the forces and moments on the blades based on Blade Element/Momentum (BEM) or Generalized Dynamic Wake (GDW) theories, including dynamic stall, tower shadow, and skewed inflow correction [24]. The Riflex nonlinear finite element solver uses a Lagrangian formulation which accounts for geometric nonlinearity using a co-rotated ghost reference, and solves the equations of motion in the time domain using Newton-Raphson iteration. The generator torque and blade pitch control system was written in Java. This combination provided a stable nonlinear finite element solver, sophisticated hydrodynamics, well-tested aerodynamics, and control logic. The Simo-Riflex wind turbine module has been previously verified [25, 26], and the Simo-Riflex-AeroDyn combination is documented in [27].

Environmental Conditions

Table 4 summarizes the four environmental conditions (ECs) considered here, which comprise directionally aligned irregular waves and turbulent wind. The four ECs shown in Table 4 are listed in order of increasing severity and represent correlated wind and wave conditions [28]. In ECs 1-3, the wind turbine generates power, while EC 4 represents a 50-year storm condition where the blades are fully feathered and the rotor is idling. It should be noted that the maximum turbine thrust force occurs in EC 2.

TABLE 4. ENVIRONMENTAL CONDITIONS

Condition	1	2	3	4
H_s (m)	2.5	3.1	4.4	12.7
T_p (s)	9.8	10.1	10.6	14.1
U (m/s)	8.0	11.4	18.0	50.0
I	0.20	0.17	0.15	0.11

The irregular waves were generated by FFT from a JONSWAP spectrum with the desired significant wave height, H_s, and peak period, T_p, using a frequency discretization of 0.002 rad/s [22]. In order to avoid unphysical first order wave excitation, the spectrum was cut above a wave cutoff frequency ω_c [29]:

$$\omega_c = \sqrt{2g/H_s} \tag{6}$$

where g is the acceleration due to gravity.

NREL's TurbSim program was used to create 3D wind fields with mean hub-height wind speed, U, and turbulence intensity, I, based on the Kaimal spectrum with the IEC Class B normal turbulence model (NTM) [30]. The wind shear was modeled by the power law with exponent 0.14 and surface roughness length 0.3 mm [31]. In the vertical plane 32x32 points were used, with wind field generation time step 0.05 seconds. Six three-hour wind and wave series for each environmental condition were applied to each of the different hydrodynamic load models.

RESPONSE IN TURBULENT WIND AND IRREGULAR WAVES

Fig. 7 compares the mean values (μ), and Fig. 8 compares the standard deviation (σ) of four response quantities for all of the TLPWT designs, hydrodynamic models, and environmental conditions. Although the standard deviation does not give a full picture of the response, it can give an indication of the effect of the different hydrodynamic models on more complete fatigue and extreme load predictions. For example, a rough prediction of the extreme value can be obtained from $\mu + k\sigma$, where k is chosen to represent a probability level. As shown in Fig. 7, all three hydrodynamic models predict similar mean values.

The surge response (ζ_1) is generally largest in the storm condition (EC 4) and in the maximum thrust condition (EC 2). There is almost no difference in the surge response due to the sum-frequency QTF, but the Morison model predicted slightly smaller $\mu(\zeta_1)$ and larger $\sigma(\zeta_1)$ than the potential flow models, particularly for larger wave heights and large diameter. The difference in motions is observed at the surge natural frequency, where there is little damping and forcing differences become more evident in the response.

The second subplot of Fig. 8 shows the pitch response ζ_5, which is small in absolute value, but important due to its implications for tendon tension variation and nacelle accelerations. The agreement between the potential flow models and the Morison model is somewhat worse for pitch compared to surge, particularly for the TLPWTs with large diameter. It is possible that the agreement could be slightly improved by varying the Morison coefficients along the length of the cylinder, but the main difference in response is at the pitch natural frequency rather than at the wave frequency. The effect of the sum-frequency forces can be seen in the storm condition, where the pitch motions increased 2-10% compared to the first order model. The sum-frequency QTF had the largest effect, by percentage, on TLPWT 2, which had a relatively deep draft, large pontoons, and low pretension.

The standard deviation of the fore-aft bending moment at the base of the wind turbine tower (M_{FA}) is presented in the third subplot of Fig. 8. The tower base bending moment increases with wave height, despite the decreased thrust between ECs 2 and 3. The second order forces have less than 2% effect on M_{FA} despite the increased pitch motions. The Morison model leads to higher load predictions (3-14% for TLPWTs 1-3) in both operational and storm conditions, primarily in the upper half the wave frequency range and around the pitch natural frequency.

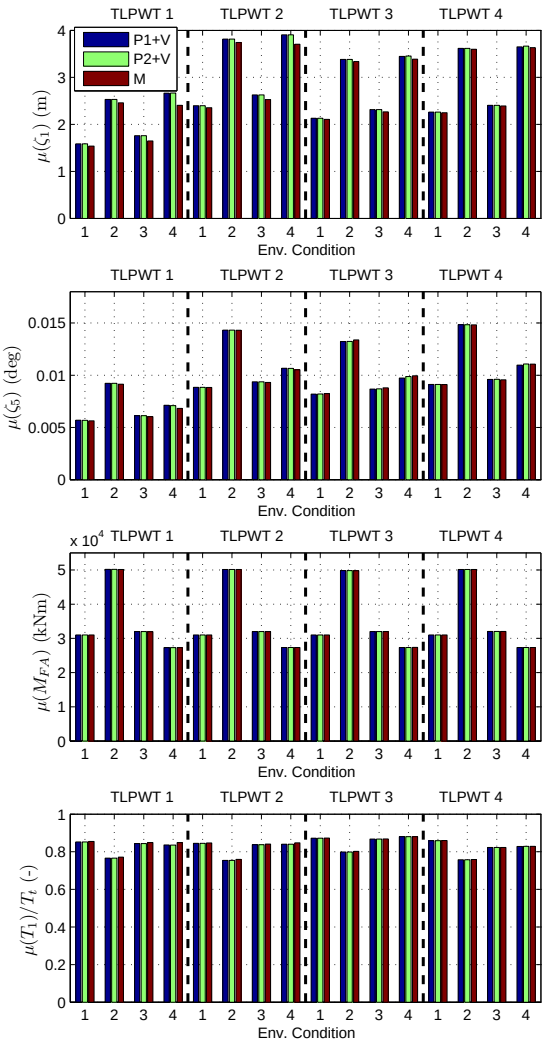

FIGURE 7. MEAN VALUE OF KEY RESPONSE INDICATORS (SURGE, PITCH,TOWER BASE FORE-AFT BENDING MOMENT, DOWNWIND TENDON TENSION)

Finally, the tendon tension variation in the downwind line (T_1) is shown in the fourth subplot of Fig. 8, as a function of the still water tension, T_t. The tendon tension is a particularly crucial consideration for TLPWTs, since slack conditions can lead to tendon disconnect and loss of the platform. Both the mean tension and tension variation should be considered in order to estimate the probability of slack (for example, $\mu - k\sigma$). The second order forces lead to 2-9% increases in the tendon tension variation in the storm conditions, while the Morison model predicts up to 25% larger tendon tension variation for TLPWT 1. The Morison model is not necessarily conservative, however: TLPWT 3 shows less tendon tension variation in the wave frequency region.

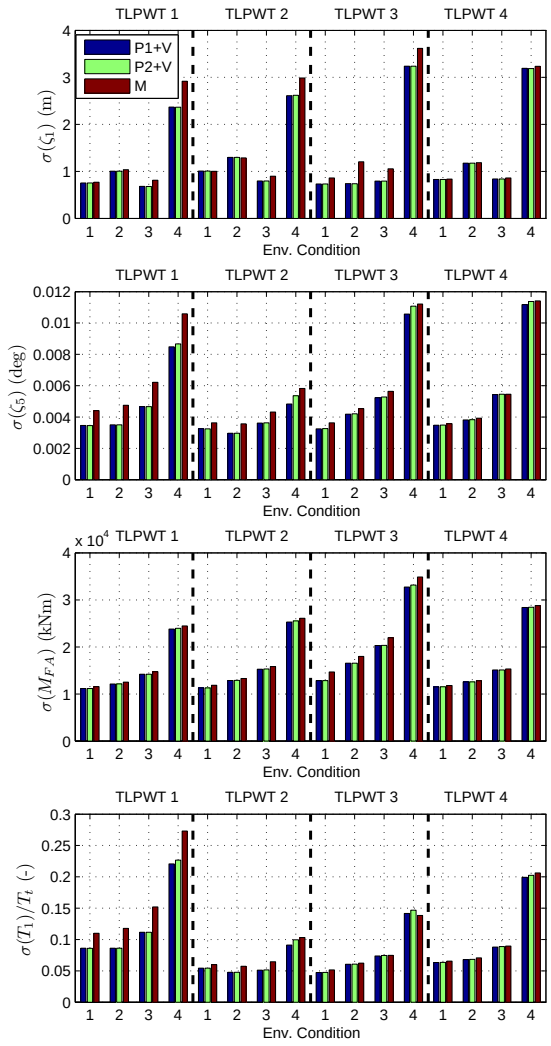

FIGURE 8. STANDARD DEVIATION OF KEY RESPONSE INDICATORS (SURGE, PITCH, TOWER BASE FORE-AFT BENDING MOMENT, DOWNWIND TENDON TENSION)

The spectra of the tendon tension variation for TLPWTs 2 and 3 are shown in Figs. 9 and 10, respectively. When the wave conditions were relatively benign, the low-frequency wind-induced response was dominant, while the response at the wave and pitch/bending natural frequency increased as the wave height increased. TLPWT 2 was very sensitive to forces near the double wave period: even the small wave excitation from the first order wave and viscous forces was sufficient to cause a response peak in the operational conditions. The Morison load formulation led to larger response above the main wave frequencies in ECs 2-4. The second order wave loads increased the high-frequency response in EC 4. TLPWT 3, in contrast, was less sensitive to wave loads near the double frequency, but showed increased response around the pitch/bend frequency.

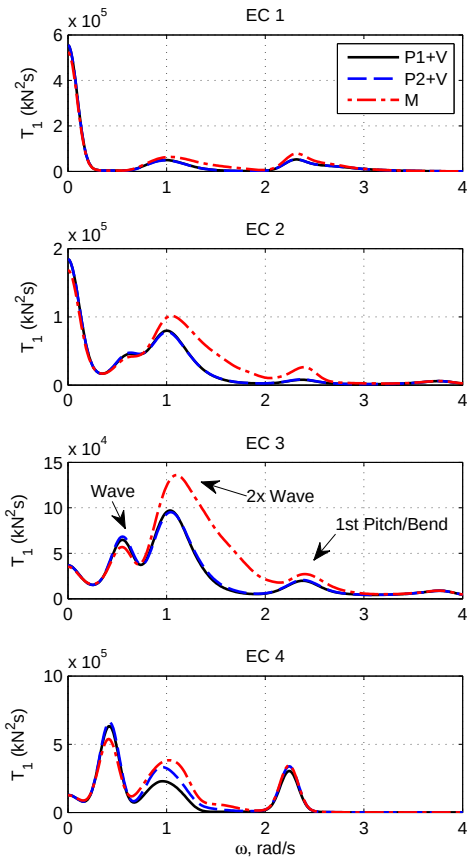

FIGURE 9. LINE 1 TENSION SPECTRA, TLPWT 2

Although the tendon tension variation for TLPWT 2 showed a large component in the double wave frequency range, the tower base fore-aft bending moment did not show a corresponding peak (Fig. 11). There was very little difference in the spectral M_{FA} responses for TLPWT 2, but increased response at the pitch/bending frequency (P2+V) or at the wave frequency (M) was more obvious for TLPWT 3 (spectra not shown).

CONCLUSIONS

Effect of Sum-Frequency Wave Forcing

Including the sum-frequency wave forcing had very little effect on the results in operational conditions, but led to increased pitch/bending motions at the natural frequency in the storm condition. Increases in the tendon tendon variation and tower base bending moment at twice the wave frequency and at the pitch/bending natural frequency were observed in the global aero-servo-hydro-elastic simulations. The tendon tension was more sensitive to second order forces than the tower bending moment, and the larger TLPWTs were more sensitive to second order forces in general. The implications for tendon fatigue were not examined here.

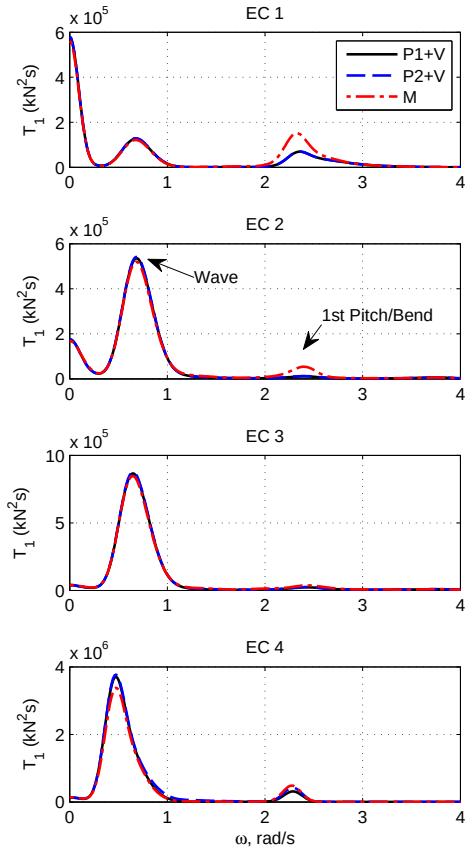

FIGURE 10. LINE 1 TENSION SPECTRA, TLPWT 3

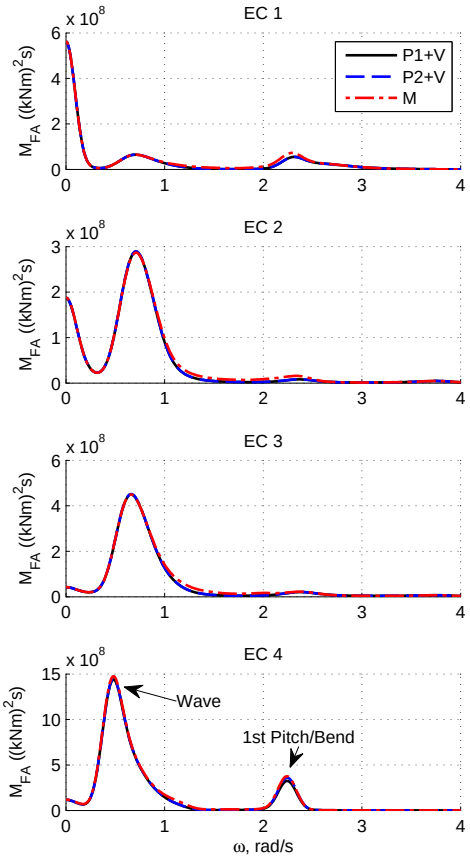

FIGURE 11. TOWER BASE FORE-AFT BENDING MOMENT SPECTRA, TLPWT 2

Use of Morison's Equation

Morison's equation gave reasonably good agreement for slender structures in operational conditions, but generally led to larger pitch moment predictions for structures with large diameter and in large waves. The Froude-Krylov force as computed by Morison's equation does not decay as quickly as the potential flow wave excitation, leading to larger (unrealistic) excitation for large wave frequencies and near the pitch/bending natural frequency. Even with the truncated wave spectrum, 10-30% disagreement in $\sigma(T_1)$ was found for TLPWTs 1 and 2.

Comparison of Model Effects for Different TLPWTs

As one might expect, TLPWT 4 (smallest) showed good agreement between Morison's equation and potential flow. The structures with relatively large pontoons were sensitive to the inclusion of sum-frequency pitch loads. Lower tendon tension led to greater sensitivity to forcing at twice the wave frequency.

The effect of the different hydrodynamic load models on pitch motions was fairly directly linked to changes in the tendon tension, but the effect on the tower fore-aft bending moment also depended on the TLPWT design. The structures studied here did not include a large range of pitch/bending natural frequencies, which may also influence how the different hydrodynamic models affect the predicted response.

ACKNOWLEDGMENT

Support for this work was provided by Statoil through an MIT-NTNU Gemini cooperative research project. The authors are grateful to MARINTEK for support in the development of the coupled computer code.

REFERENCES

[1] Butterfield, S., Musial, W., Jonkman, J., Sclavounous, P., and Wayman, L., 2005. "Engineering challenges for floating offshore wind turbines". In 2005 Copenhagen Offshore Wind Conference, no. NREL/CP-500-38776.

[2] Robertson, A. N., and Jonkman, J. M., 2011. "Loads analysis of several offshore floating wind turbine concepts". In 21st International Society of Offshore and Polar Engineers Conference, no. NREL/CP-5000-50539.

[3] Sclavounos, P., Lee, S., DiPietro, J., Potenza, G., Caramuscio, P., and Michele, G. D., 2010. "Floating offshore wind

turbines: tension leg platform and taught leg buoy concepts supporting 3-5 MW wind turbines". In European Wind Energy Conference EWEC 2010, Warsaw, Poland.

[4] Fulton, G., Malcolm, D., Elwany, H., Stuart, W., Moroz, E., and Dempster, H., 2007. Semi-submersible platform and anchor foundation systems for wind turbine support. Tech. Rep. NREL/SR-500-40282, National Renewable Energy Laboratory.

[5] Matha, D., 2009. "Model development and loads analysis of an offshore wind turbine on a tension leg platform, with a comparison to other floating turbine concepts". Master's thesis, University of Colorado-Boulder, April.

[6] Matha, D., Fischer, T., Kuhn, M., and Jonkman, J., 2010. "Model development and loads analysis of a wind turbine on a floating offshore tension leg platform". No. NREL/CP-500-46725.

[7] Stewart, G., Lackner, M., Robertson, A., Jonkman, J., and Goupee, A., 2012. "Calibration and validation of a fast floating wind turbine model of the deepcwind scaled tension-leg platform". In 22nd International Offshore and Polar Engineering Conference, no. NREL/CP-5000-54822.

[8] Moon III, W. L., and Nordstrom, C. J., 2010. "Tension leg platform turbine: A unique integration of mature technologies". In Proceedings of the 16th Offshore Symposium, Texas Section of the Society of Naval Architects and Marine Engineers, pp. A25–A34.

[9] Henderson, A. R., Argyriadis, K., Nichos, J., and Langston, D., 2010. "Offshore wind turbines on TLPs - assessment of floating support structures for offshore wind farms in german waters". In 10th German Wind Energy Conference, Bremen, Germany.

[10] Nihei, Y., Matsuura, M., Fujioka, H., and Suzuki, H., 2011. "An approach for the optimum design of TLP type offshore wind turbines". In 30th International Conference on Ocean, Offshore, and Arctic Engineering, no. OMAE2011-50258.

[11] Copple, R. W., and Capanoglu, C., 2012. "Tension leg wind turbine conceptual design suitable for a wide range of water depths". In 22nd International Ocean and Polar Engineering Conference, Vol. 1, pp. 396–403.

[12] Faltinsen, O., 1990. *Sea Loads on Ships and Offshore Structures*. Cambridge University Press.

[13] Kvittem, M. I., Bachynski, E. E., and Moan, T., 2012. "Effects of hydrodynamic modelling in fully coupled simulations of a semi-submersible wind turbine". *Energy Procedia,* ***24***, pp. 351–362.

[14] Faltinsen, O. M., 1990. "Wave loads on offshore structures". *Annual Review of Fluid Mechanics,* ***22***, pp. 35–56.

[15] Kim, M. H., and Yue, D. K. P., 1988. "The nonlinear sum-frequency wave excitation and response of a tension-leg platform". In Intl. Conference on Behaviour of Offshore Structures (BOSS '88), Vol. 2: Hydrodynamics, pp. 687–703.

[16] Roald, L., Jonkman, J., Robertson, A., and Chokani, N., 2013. "Effect of second-order hydrodynamics on floating offshore wind turbines". In 10th Deep Sea Offshore Wind R&D Conference. (oral presentation).

[17] Bachynski, E. E., and Moan, T., 2012. "Design considerations for tension leg platform wind turbines". *Marine Structures,* ***29***, pp. 89–114.

[18] Det Norske Veritas, 2010. *Wadam User Manual*, 8.1 ed., January.

[19] Herfjord, K., and Nielsen, F. G., 1986. "Non-linear wave forces on a fixed vertical cylinder due to the sum frequency of waves in irregular seas". *Applied Ocean Research,* ***8***(1), pp. 8–21.

[20] Lee, C.-H., J. N. Newman, M.-H. K., and Yue, D. K. P., 1991. "The computation of second-order wave loads". In Offshore Mechanics and Arctic Engineering Conference.

[21] Det Norske Veritas, 2010. Global performance analysis of deepwater floating structures. Tech. Rep. DNV-RP-F205.

[22] MARINTEK, 2011. *SIMO User's Manual*.

[23] MARINTEK, 2011. *RIFLEX User's Manual*.

[24] Moriarty, P. J., and Hansen, A. C., 2005. AeroDyn theory manual. Tech. Rep. NREL/TP-500-36881.

[25] Ormberg, H., Passano, E., and Luxcey, N., 2011. "Global analysis of a floating wind turbine using an aero-hydro-elastic model: Part 1: Code development and case study". In 30th International Conference on Ocean, Offshore, and Arctic Engineering, no. OMAE2011-50114.

[26] Luxcey, N., Ormberg, H., and Passano, E., 2011. "Global analysis of a floating wind turbine using an aero-hydro-elastic numerical model. Part 2: Benchmark study". In 30th International Conference on Ocean, Offshore, and Arctic Engineering, no. OMAE2011-50088.

[27] Ormberg, H., and Bachynski, E. E., 2012. "Global analysis of floating wind turbines: Code development, model sensitivity and benchmark study". In 22nd International Ocean and Polar Engineering Conference, Vol. 1, pp. 366–373.

[28] Johannessen, K., Meling, T. S., and Haver, S., 2001. "Joint distribution for wind and waves in the northern North Sea". In The 11th International Offshore and Polar Engineering Conference & Exhibition, International Society of Offshore and Polar Engineers.

[29] Det Norske Veritas, 2010. Environmental conditions and environmental loads. Tech. Rep. DNV-RP-C205, October.

[30] International Electrotechnical Commission, 2005. Wind turbines: Part 1: Design requirements. Tech. Rep. IEC61400-1:2005(E).

[31] International Electrotechnical Commission, 2009. Wind turbines: Part 3: Design requirements for offshore wind turbines. Tech. Rep. IEC61400-3.